MATERIALS CHEMISTRY FRONTIERS

RESEARCH ARTICLE

View Article Online
View Journal | View Issue



Cite this: *Mater. Chem. Front.*, 2023, 7, 2436

# Pseudo single lithium-ion conductors enabled by a metal–organic framework with biomimetic lithium-ion chains for lithium metal batteries†

Jian-Qiang Shen,[ab] Ying-Li Song,[a] Chun-Ting He,[c] Chen Zhang,[b] Xing Lu,[b] Zhikai Qi,[a] Yunfeng Lu *[b] and Xian-Ming Zhang *[ad]

Received 13th January 2023,
Accepted 4th March 2023

DOI: 10.1039/d3qm00044c

rsc.li/frontiers-materials



The development of new and efficient, non-precious metal-based single lithium-ion conductors is one of the premier challenges in lithium metal batteries (LMBs). Inspired by the biologic proton chains, we designed pseudo single lithium-ion conductors (PSLICs) by immobilizing liquid electrolytes in a unique Zr-carboxylate framework. Such unique PSLIC contains biomimetic lithium ion chains and exhibits high lithium ionic conductivity (0.35 mS $cm^{-1}$) and low activation energy (0.19 eV). As illustrated by density functional theory calculations, single lithium ion chains can be formed within PSLIC, and lithium ions can be transported by jumping between solvents and anions. $LiFePO_4$|Li cell with such PSLIC exhibits significantly extended cycling life (>900 cycles) with 77% capacity retention and improved Coulombic efficiency (>97%).

## Introduction

Lithium metal is a promising anode material due to its high theoretical capacity (3860 mA h $g^{-1}$) and the lowest electrochemical potential (−3.04 V *vs.* standard hydrogen electrode).[1–3] However, the safety concern raised from the growth of lithium dendrites and the poor electrochemical performance associated with low Coulombic efficiency greatly restrict the applications of lithium metal batteries (LMBs).[4,5] In contrast to current strategies, *i.e.*, adding electrolyte additives and establishing a surface protective layer, the replacement of liquid electrolytes with single lithium-ion conductors (SLICs) is one of the most effective strategies.[6,7] In general, SLICs with high Li-ion transference numbers are well-acknowledged to have advantages over conventional dual-ion conducting electrolytes, especially in LMBs.[8,9] SLICs are categorized into two groups: ceramic SLICs and polymeric SLICs. Although ceramic SLICs present high Li-ion conductivity,[10,11] such as $Li_7La_3Zr_2O_{12}$ (0.51 mS $cm^{-1}$),[12] $Li_7P_3S_{11}$ (3.2 mS $cm^{-1}$),[13] and $Li_{10}GeP_2S_{12}$ (12 mS $cm^{-1}$),[14] they generally suffer from large interfacial resistance and unsatisfactory electrochemical stability against metallic lithium.[15] Polymeric SLICs can covalently bond with anions to the polymer backbones to immobilize them.[9,16] However, the requirements for strong mechanical properties and high Li-ion conductivity of polymeric SLICs are contradictory and hard to be balanced.[8,15]

Considering the challenges for SLICs, metal–organic frameworks (MOFs), with extraordinary porosity, electrical insulation, and versatile functional tunability with precision at the molecular level, offer a broad choice of SLICs for LMBs.[17,18] Taking these advantages, some MOF-based SLICs have been constructed by dative modification and covalent modification.[18–23] For example, Long and Dinca *et al.* fixed the *tert*-butyl lithium and halogenated lithium onto the open metal sites (OMSs) of $[Zn_2(dobdc)(H_2O)_2]$ (MOF-74-Zn, $H_4$dobdc = 2,5-dihydroxyterephthalic acid) and $((CH_3)_2NH_2)[Cu_2(btdd)Cl_3]$ (MIT-20, $H_2$btdd = bis(1*H*-1,2,3-triazolo-[4,5-*b*],[4′,5′-*i*])dibenzo[1,4]dioxin), respectively, and obtained a series of dative modification-SLICs.[18–20] To expand the applications of MOF-based SLICs in batteries, our group designed a series of MOF-based electrolytes by fixing the $LiClO_4$ onto the OMSs of $[Cu_3(BTC)_2(H_2O)_3]$ (HKUST-1, $H_3$BTC = 1,3,5-benzenetricarboxylic acid), $[Zr_6O_4(OH)_4(BPDC)_6]$ (UiO-67, $H_4$BPDC = biphenyl-4,4-dicarboxylic acid), and $[M_3O(BTC)_2(H_2O)_2X_3]$ (MIL-100, M = Al, Cr, Fe; X = $F^-$, $OH^-$).[17] However, it is necessary to further optimize the structures and properties of materials to achieve satisfactory electrochemical performance.

[a] *Key Laboratory of Magnetic Molecules & Magnetic Information Materials, Ministry of Education, School of Chemistry & Material Science, Shanxi Normal University, Taiyuan, 030006, P. R. China. E-mail: zhangxm@dns.sxnu.edu.cn*
[b] *Department of Chemical and Biomolecular Engineering, University of California, Los Angeles, CA, 90095, USA. E-mail: luucla@ucla.edu*
[c] *Key Laboratory of Functional Small Organic Molecule, Ministry of Education, College of Chemistry and Chemical Engineering, Jiangxi Normal University, Nanchang, 330022, P. R. China*
[d] *School of Chemistry, Taiyuan University of Technology, Taiyuan, 030024, P. R. China*

† Electronic supplementary information (ESI) available. See DOI: https://doi.org/10.1039/d3qm00044c

 

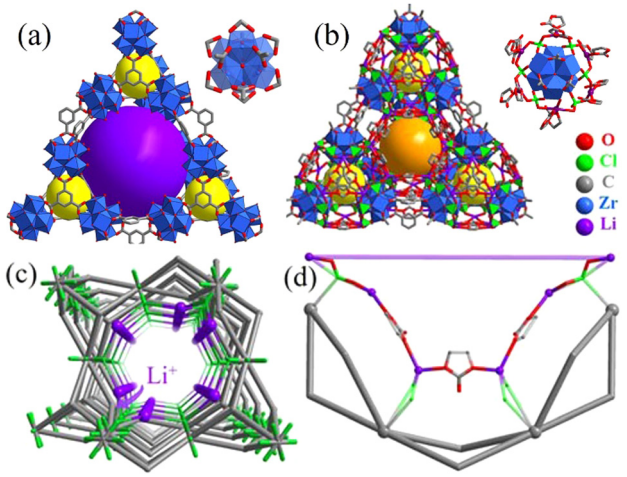


Fig. 1 (a) Structure of **808** made from the trigonal prismatic $[Zr_6(\mu_3\text{-}O)_8(O)(RCOO)_6(FA)_6]$ clusters and trigonal $BTC^{3-}$ ligands with pore channels of 18 Å. (b) Structure of **808-LCE** made from the trigonal prismatic $[Li(EC)_2]_6[Zr_6(\mu_3\text{-}O)_8(O)(RCOO)_6(ClO_4)_6]$ clusters and trigonal $BTC^{3-}$ ligands with pore channels of 6 Å. (c) Schematic of single-file lithium ion chains (purple dots) in the **808-LCE** scaffold (dark gray) with bound $X^-$ ions (green dots), enabling fast transport of $Li^+$ ions in the single lithium ion channels. (d) Single lithium-ion chain in **808-LCE** and lithium ions can be transported by jumping between solvents and anions.

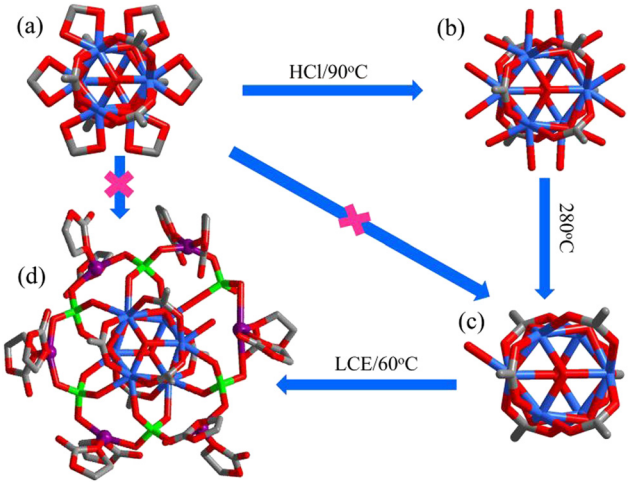


Scheme 1 Post-synthesis transformation of hexa-nuclear zirconium clusters from **808** (a), **808-OH** (b), **808-O** (c), to **808-LCE** (d).

In biological systems, the transport of protons generally involves proton channels, a class of protein molecules embedding single-file water chains as highly effective proton conducting wires.[24] Inspired by the biologic proton chains, we report a novel biomimetic pseudo SLICs of $Li_6[Zr_6(\mu_3\text{-}O)_8O(BTC)_2(ClO_4)_6]\cdot 16EC$ (**808-LCE**) by immobilizing $LiClO_4\cdot 2EC$ (**LCE**, Fig. S1, ESI†) in a unique Zr-carboxylate framework. The PSLIC contains single-file lithium-ion chains (Fig. 1), which exhibit high lithium ionic conductivity (0.35 mS $cm^{-1}$) and low activation energy (0.19 eV) simultaneously. Prototype, $LiFePO_4$|Li cell with the SLIC exhibits significantly extended cycling life (>900 cycles) with 80% capacity retention and improved Coulombic efficiency (>97%). Our work not only provides a new strategy to bridge the gap between liquid electrolytes and solid electrolytes but also opens a new route for designing novel SLICs for all-solid-state LMBs.

## Results and discussion

### Synthesis and characterization

A schematic illustration of the construction of the MOF-based SLIC is shown in Scheme 1, in which **808-LCE** was formed by functionalizing $[Zr_6(\mu_3\text{-}O)_4(\mu_3\text{-}OH)_4(BTC)_2(FA)_6]$ (**808**, HFA = formic acid) with **LCE** through dative modification. **808** is a 3,6-connencted three-dimensional framework with an overall spn topology and built up by the trigonal-prismatic $[Zr_6(\mu_3\text{-}O)_4(\mu_3\text{-}OH)_4(RCOO)_6(FA)_6]$ clusters and trigonal $BTC^{3-}$ ligands (Fig. 1a and Fig. S2a, ESI†). This kind of arrangement of these clusters gives rise to one octahedral cavity (with an internal pore diameter of 18.4 Å) and four tetrahedral cavities (with an internal pore diameter of 4.8 Å) per MOF formula unit (Fig. S2a, ESI†). The coordination framework of **808** defines one-dimensional (1D) linear channel system with a large pore size (18.4 Å, Fig. S2b, ESI†). Besides the high surface area and large cavity size, **808** also presents high chemical/electrical stability and high potential open metal site (OMSs) density.[25,26] Therefore, **808** could be a good option for constructing SLICs with high ionic conductivity.

**808** was obtained by solvothermal reaction of $ZrOCl_2$, $H_3BTC$, and HFA in *N*,*N*-dimethylacetamide, according to the literature.[25,27] Then, the formate groups in its framework were transformed to $H_2O/OH^-$ in 1 M HCl (90 °C, 12 h)[26,27] and obtain $[Zr_6(\mu_3\text{-}O)_4(\mu_3\text{-}OH)_4(BTC)_2(OH)_6(H_2O)_6]$. Moreover, its TG and VTPXRD (Fig. S3 and S4, ESI†) show that the coordinated water molecules and $OH^-$ could be removed at 250 °C, and the framework with 11 OMSs per building block was subsequently derived: $[Zr_6(\mu_3\text{-}O)_8O(btc)_2]$ (**808-O**, Scheme 1c, Fig. S2b and e, ESI†). Then, the microcrystal powders of **808-LCE** were obtained by a further post-synthetic reaction of **808-O** with **LCE** in the glove box.

In principle, as a structural analogue of $SO_4^{2-}$, the $ClO_4^-$ cross-linked hybrid MOF **808-LCE** should be in isomorphism with $[Zr_6O_5(OH)_3(BTC)_2(SO_4)_{2.5}(H_2O)_{2.5}]$ except that the metal cluster nodes are changed into $[Li(EC)_2]_6[Zr_6(\mu_3\text{-}O)_8(O)(RCOO)_6(ClO_4)_6]$ (Fig. 1b, Fig. S2c and f, ESI†). On this basis, the structure of **808-LCE** was simulated by Material Studio. As shown in Fig. 1b, **808-LCE** also has two kinds of cages and can be simplified to 3,6-connected spn topology. Compared to **808**, the pore size of the 1D linear channel has been reduced to 6 Å because some channels are occupied by coordination guest molecules. In the cluster of $[Li(EC)_2]_6[Zr_6(\mu_3\text{-}O)_8(O)(RCOO)_6(ClO_4)_6]$ (Scheme 1d), every two adjacent lithium ions are connected by $ClO_4^-$ (with a Li–Li distance of 6.1 Å) and form a six-membered ring. Moreover, six adjacent lithium ions along the channel are connected by two $ClO_4^-$ and three EC (with a Li–Li distance of 6.7 Å and 8.0 Å) and form single-file lithium chains along the channel, as shown in Fig. 1d.[25] By virtue of the high stability of **808** scaffolds and the single-file lithium chains along the channel, **808-LCE** may be a good candidate for highly

conductive SILC. In contrast, we also synthesized $6LiClO_4 \cdot 12EC@[Zr_6(\mu_3\text{-}O)_4(\mu_3\text{-}OH)_4(BTC)_2(FA)_6]$ (**LCE@808**), in which **LCE** have no coordination with the **808** scaffolds and only exists in the channel as guest molecules. As Shown in Fig. 2a, b, and Fig. S5c (ESI†), **808-LCE** and **LCE@808** have similar morphology and powder diffraction peaks.

To verify our conjecture, the Raman spectrum of **808-LCE** was probed. Raman spectrum of **808-LCE** (Fig. 2c) illustrates two characteristic peaks at 675 and 1240 $cm^{-1}$, which can be attributed to the monodentate coordination of $ClO_4^-$ and metal center.[28] Meanwhile, two characteristic peaks at 860 and 1110 $cm^{-1}$ were observed, which can be assigned to the bidentate coordination of $ClO_4^-$ and metal center.[29] We further investigated the coordination mode of **808-LCE** with DFT calculations, indicating that the $ClO_4^-$ ions should be coordinated with **808** in monodentate and bidentate modes (Fig. S6, ESI†). The binding between $ClO_4^-$ and Zr in **808-LCE** is similar to that of isomorphism in $[Zr_6O_5(OH)_3(BTC)_2(SO_4)_{2.5}(H_2O)_{2.5}]$[25] and inorganic compound $Zr(ClO_4)_4$. In contrast, there is one characteristic peak of ionic $ClO_4^-$ (935 $cm^{-1}$) in the Raman spectrum of **LCE@808** (Fig. 2c). These results indicate that perchlorates have no coordination with the frameworks of **808** and only exist in the channel as guest molecules.

Inductively coupled plasma atomic emission spectroscopy (ICP-AES, Table S1, ESI†) illustrates Li/Zr ratio of 0.99 and 1.04 in **808-LCE** and **LCE@808**, which are in good agreement with the theoretical value of 1. The content of EC within **808-LCE** and **LCE@808** is estimated by TGA (Fig. S3, ESI†), which gives a formula of **808-LCE** as $Li_6[Zr_6(\mu_3\text{-}O)_8O(BTC)_2(ClO_4)_6] \cdot 16EC$ and **LCE@808** as $6[Li(EC)_2ClO_4]@[Zr_6(\mu_3\text{-}O)_4(\mu_3\text{-}OH)_4\ (BTC)_2(FA)_6]$. In addition, the $N_2$ adsorption/desorption isotherms show that **808-LCE** partially and irreversibly collapses after the guest removal (Fig. 2d). However, **LCE@808** can retain its open frameworks after the removal of guest molecules (Fig. 2d), similar to **808**. The different thermal stabilities between **LCE@808** and **808-LCE** can be explained by the strong interaction between **LCE** and **808** scaffolds. Scanning electron microscopy (SEM) images (Fig. 2a and Fig. S5, ESI†) show similar crystalline sizes of 500 nm and morphology for **808**, **808-LCE**, and **LCE@808** particles.

## The ionic conductivities

The ionic conductivities were measured with powder pellets using alternating current impedance spectroscopy. As shown in Fig. 3a and Fig. S7 (ESI†), **808-LCE** exhibits ionic conductivity of 0.55 mS $cm^{-1}$ at 25 °C. Furthermore, the activation energy for ion transport was determined by collecting variable-temperature alternate current impedance data between 25 and 70 °C. As shown in Fig. 3b, their activation energies ($E_a$) fall in the range of 0.19 eV, which is only slightly higher than that of $LiClO_4$ liquid electrolyte (0.10 eV, Table S2, ESI†). Considering the mechanical strength requirement of solid electrolytes for LMBs, we also tested the ionic conductivities of MOF-based electrolyte films with 30% poly (vinylidene fluoride-*co*-hexafluoropropylene) (PVDF-HFP).[30] As shown in Fig. 3c and Fig. S8 (ESI†), MOF particles are uniformly distributed in the film. The ionic conductivity of the **808-LCE** film is 0.54 mS $cm^{-1}$ and its $E_a$ is 0.16 eV. Such values are close to those of **808-LCE**, indicating that the addition of polymers does not change the intrinsic characteristics of MOF-based SLICs.

Lithium-ion transport number ($t_{Li^+}$), which is the fraction of the total electrical current carried by $Li^+$, is evaluated with the potentiostatic polarization method. As shown in Fig. 3d and Fig. S10 (ESI†), the $t^+$ of **808-LCE** is 0.64, which is significantly higher than that of liquid lithium-ion electrolytes (typically less than 0.3).[31] Besides, it exhibits a high lithium-ion conductivity of 0.35 mS $cm^{-1}$. Such lithium ionic conductivity is higher than most SILCs except for some electrochemically unstable sulfide (Table S3, ESI†).[8,9,15,18,19,32–36] We also measured the ionic

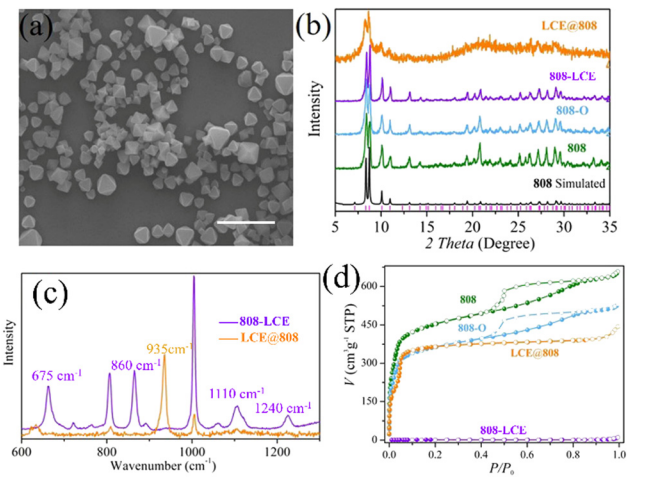


Fig. 2 (a) SEM image of **808-LCE** (scale bar 2 um). (b) PXRD of **808**, **808-O**, **808-LCE**, and **LCE@808**. (c) Raman spectra of **808-LCE** and **LCE@808**. (d) $N_2$ adsorption (solid) and desorption (open) isotherms of **808**, **808-O**, **808-LCE**, and **LCE@808** at 77 K.

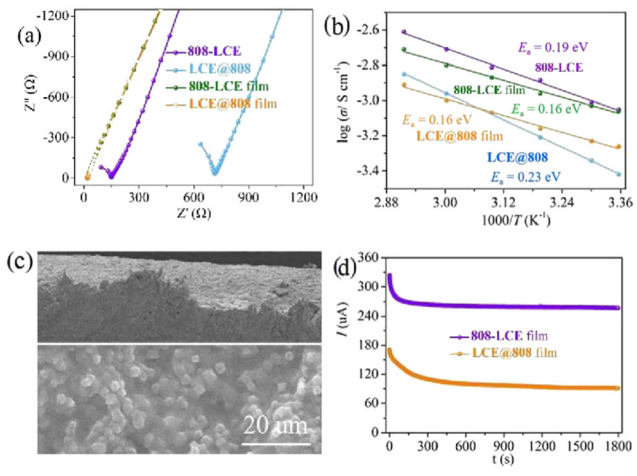


Fig. 3 (a) Nyquist plots of **808-LCE**, **LCE@808**, **808-LCE** film, and **LCE@808** film at 25 °C. (b) Arrhenius plots of various MOF-based electrolytes and their calculated activation energies for lithium-ion conduction. (c) SEM images of the **808-LCE** film (top: cross-sectional view, bottom: surface view). (d) Current-time profile for Li|MOF-SEs|Li cell at 20 mV of polarization.

 

conductivity and $t^+$ of **LCE@808** film. As shown in Fig. S8 (ESI†), **808-LCE** film and **LCE@808** film have similar morphology. Compared to **808-LCE** film, **LCE@808** film also exhibits high ionic conductivity of 0.48 mS cm$^{-1}$ (Fig. 3a and Fig. S9, ESI†), but lower $t^+$ and even only 0.27, (Fig. 3d and Fig. S10, ESI†) and lower $Li^+$ conductivity of 0.133 mS cm$^{-1}$. These results indicate that the coordination of $ClO_4^-$ with OMSs of MOFs not only improves the lithium-ion transport but also improves the lithium ionic conductivity.

### Electrochemical performance of lithium metal battery

To verify the feasibility of **808-LCE** as electrolytes for LMBs, the cyclic voltammetry (CV) of Li|**808-LCE**|SS was performed from −0.2 to 5 V (*vs.* Li/Li$^+$). As shown in Fig. 4a, **808-LCE** exhibits wide working voltage windows (−0.2 to 4.2 V), which is similar to **LCE@808** film. Compared to other MOF-based solid electrolytes, the working voltage of **808-LCE** is wider, which can be attributed to the higher chemical stability of **808** than other MOFs.[17,18,36]

Symmetric cell configuration is employed to evaluate the electrochemical stability between Li-metal anodes and MOF-based solid electrolytes. Li stripping and plating experiments were conducted under 500 μA cm$^{-2}$ and 500 μA h cm$^{-2}$ (Fig. 4b). Under a current density of 500 μA cm$^{-2}$, **LCE@808** film based symmetric cells show rapidly increased and fluctuated overpotential due to the reactions between the lithium and **LCE@808** film, while **808-LCE** film based symmetric cells present an initial overpotential of 100 mV and maintain stable electrochemical behavior for 1000 h (corresponding to 500 cycles of lithium plating/stripping).

Replacing the graphite anodes in conventional lithium-ion batteries with lithium metal anodes would dramatically increase their energy density. As a proof-of-concept, |Li cells were constructed and cycled at 0.5C (1C = 175 mA h g$^{-1}$). Using MOF-based SLIC of **808-LCE**, $LiFePO_4$|Li cell exhibits improved electrochemical kinetics and alleviated polarization, evidenced by the voltage difference between charge and discharge plateaus (100 *vs.* 110 mV) and an increased initial capacity (135 *vs.* 125 mA h g$^{-1}$) (Fig. 4c). After 1000 cycles, the cells with **808-LCE** based electrolytes exhibit a reversible capacity of 103.6 mA h g$^{-1}$ and a capacity retention of 77%, while the cell with **LCE@808** film electrolytes suffers from rapid deterioration with a capacity retention of 50% (Fig. 4d).

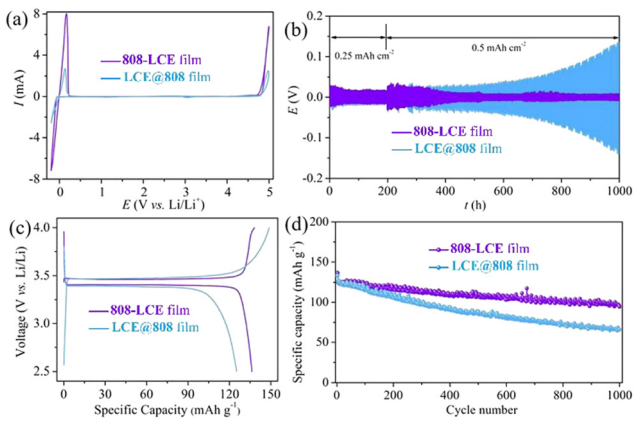


Fig. 4 Electrochemical performance of lithium metal anodes. (a) Cyclic voltammetry (CV) profiles of **808-LCE** film and **LCE@808** film. (b) Voltage profiles of symmetric lithium cells for **808-LCE** film and **LCE@808** film at 0.50 mA cm$^{-2}$. (c) Voltage-capacity profile of $LiFePO_4$|Li cells for **808-LCE** film and **LCE@808** film during the third cycle at 0.5 mA h cm$^{-2}$. (d) Galvanostatic cycling performance of $LiFePO_4$|Li cells for **808-LCE** film and **LCE@808** film at 0.5 mA h cm$^{-2}$.

To further understand the mechanism, the solid electrolyte interfaces (SEIs) were investigated using SEM and electrochemical impedance spectroscopy (EIS). The EIS of the $LiFePO_4$|Li cell shows a similar and low charge transfer resistance of 100 Ω for **808-LCE** film after 1 cycle and 100 cycles (Fig. S11, ESI†). In contrast, the impedance of the cell with **LCE@808** film increases dramatically after 100 cycles although it shows lower charge transfer resistance of 80 Ω after 1 cycle. Meanwhile, the SEI layer of the battery using **808-LCE** film as electrolyte is still very compact and uniform while that of the battery using **LCE@808** film as electrolyte is very rough (Fig. S12, ESI†) after 100 cycles. The improved cycling life indicates that the coordination of $ClO_4^-$ and OMSs of MOFs possesses superb electrochemical stability and capability to reduce side reactions.

## Experimental

For a comprehensive description of analytical methods and experimental procedures, the reader is referred to the ESI.† An overview of the central syntheses is provided here.

### Synthesis of $[Zr_6(\mu_3\text{-}O)_4(\mu_3\text{-}OH)_4(BTC)_2(FA)_6]$·guest (denoted as MOF-808 or 808)

A mixture of $ZrCl_4$ (0.699 g, 3.0 mmol), $H_3btc$ (1,3,5-benzenetricarboxylic acid, 0.420 g, 2.0 mmol), formic acid (50 mL), and *N*,*N*-dimethylformamide (DMF, 50 mL) was stirred for 30 min in air, then transferred into a 100 mL vial and sealed with a screw cap, which was heated in an oven at 120 °C for 48 h, and then cooled to room temperature at a rate of 10 °C h$^{-1}$, giving white microcrystalline powders (yield 50%).

### Synthesis of $[Zr_6(\mu_3\text{-}O)_4(\mu_3\text{-}OH)_4(BTC)_2(OH)_6(H_2O)_6]$·guest (denoted as 808-OH)

500 mg of microcrystalline **MOF-808-FA** in 50 mL 1 M HCl was heated at 90 °C for 12 h and then cooled to room temperature at a rate of 10 °C h$^{-1}$, and the resultant microcrystalline powders were washed with acetone three times and finally filtered and dried under vacuum (yield 52%). These microcrystalline powders were heated in a shrek bottle at 250 °C for 24 h under vacuum to obtain activated samples $[Zr_6(\mu_3\text{-}O)_8O(BTC)_2]$ (denoted as **808-O**) and kept in the glove box for reserve.

### Synthesis of $Li_6[Zr_6(\mu_3\text{-}O)_8O(BTC)_2(ClO_4)_6]$·16EC (denoted as 808-LCE)

A mixture of **808-O** (1106 mg, 1.0 mmol), $LiClO_4$ (1915 mg, 18 mmol), and ethylene carbonate (EC, 19 mL) was heated at 60 °C for 72 h and then cooled to room temperature; the

resultant reddish brown microcrystalline powders were washed with solvent three times and then immersed in the solvent for 24 h, and finally filtered and dried (yield 46%). Notice: all the experiments must be carried out in the glove box. EA calc. (%) for $Li_6[Zr_6(\mu_3\text{-}O)_8O(BTC)_2(ClO_4)_6]\cdot 16EC$ ($C_{66}H_{70}Li_6O_{93}Cl_6Zr_6$): C, 25.14; H, 2.24; found: C, 25.09; H, 2.32. A Zr/Li ratio of 0.99 was determined by ICP-AES.

### Synthesis of $6[Li(EC)_2ClO_4]@[Zr_6(\mu_3\text{-}O)_4(\mu_3\text{-}OH)_4(BTC)_2(FA)_6]$ (denoted as LCE@808)

A mixture of **808** (1364 mg, 1.0 mmol), $LiClO_4$ (1915 mg, 18 mmol), and ethylene carbonate (EC, 19 mL) was heated at 60 °C for 72 h and then cooled to room temperature; the resultant reddish brown microcrystalline powders were washed with solvent three times and then immersed in the solvent for 24 h, and finally filtered and dried (yield 46%). Notice: All the experiments must be carried out in the glove box. EA calc. (%) for $6[Li(EC)_2ClO_4]@[Zr_6(\mu_3\text{-}O)_4(\mu_3\text{-}OH)_4(BTC)_2(FA)_6]$ ($C_{60}H_{64}Li_6O_{92}Cl_6Zr_6$): C, 23.56; H, 2.11; found: C, 23.69; H, 2.16. A Zr/Li ratio of 1.04 was determined by ICP-AES.

### Preparation of 808-LCE film and LCE@808 film

**808-LCE** and **LCE@808** films were prepared by homogenously mixing 320 mg of MOFs (**808-LCE** and **LCE@808**) with 160 mg of P(VdF-HFP) powders in 5 mL of dimethyl carbonate (DMC) and 1 mL of ethylene carbonate (EC) for 24 h (ambient temperature).

### Electrochemical studies

CV tests (Biologic VMP3) were conducted in coin-cell configuration with a scan rate of 1.0 mV $s^{-1}$ between −0.2 and 5.0 V, where lithium chips were utilized as reference/counter electrodes, and stainless-steel plates were used as the working electrodes.

The ionic conductivity was measured using EIS after placing the pellets/films between two stainless steel blocking contacts in a 2032-type coin cell. The frequency range was from 106 to 1 Hz, and AC amplitude was 100 mV. Ionic conductivity ($\sigma$, S $cm^{-1}$) was determined by using the end point of the semicircle as the ionic resistivity ($R$, Ohm), thickness ($L$, cm), and area of the pellet ($A$, $cm^2$) based on $\sigma = L/(R \times S)$. To measure the activation energies, conductivity was measured at different temperatures and calculated based on the Arrhenius relation with a linear fitting coefficient over 0.99.

Determination of $t_{Li^+}$ was performed through the combined measurement of alternating-current (AC) impedance and potentiostatic polarization. The time dependence of the current was detected *via* Li|Li symmetric cell with an applied voltage of 20 mV ($\Delta V$), during which the initial current ($I_0$) was monitored until reaching the steady-state current ($I_{ss}$). The same cell was monitored to measure the resistance of the electrolyte and the electrolyte-Li metal interface by EIS before ($R_0$) and after ($R_{ss}$) ($10^6$ to 1 Hz, 10 mV amplitude) applying the voltage. $t_{Li^+}$ can be calculated with the following expression: $t_{Li^+} = I_{ss}(\Delta V - I_0R_0)/I_0(\Delta V - I_{ss}R_{ss})$.

Li stripping and plating tests were performed using Li|Li cells by galvanostatically charging and discharging (Landt instrument) for a period of 2 h each at a current density of 0.5 mA $cm^{-2}$, except for the initial 100 cycles at 0.25 mA $cm^{-2}$.

Prototype batteries were fabricated by assembling a conventional $LiFePO_4$ cathode (2 mg $cm^{-2}$) and a Li anode (760/50 μm) in coin cells (2.5 to 4 V *vs.* $Li/Li^+$ for $LiFePO_4$). The $LiFePO_4$ cathodes were prepared by homogenously blending $LiFePO_4$ (MTI), acetylene black, and polyvinylidene difluoride (PVdF) at a ratio of 8 : 1 : 1 in *N*-methyl-2-pyrrolidone (NMP). The resulting slurry was uniformly coated on a conductive carbon-coated Al foil and dried in a vacuum oven at 90 °C for 12 h. The specific capacity is calculated based on the active materials in the cathode. 1C charging and discharging rate here is defined as 175 mA $g^{-1}$. All the electrochemical tests were carried out at ambient temperature (25 °C) unless specified.

## Conclusions

In summary, we report a class of pseudo SLICs with biomimetic lithium ion chains by immobilizing the liquid electrolytes in a unique Zr-carboxylate framework. By using this SILC, the Coulombic efficiency and cycling stability for LMBs are significantly improved, and 80% capacity of $LiFePO_4$|Li cells is retained after 900 cycles. This work not only provides a new strategy to bridge the gap between liquid electrolytes and solid electrolytes but also opens a new route for using biomimetic concepts for designing novel SLICs for all-solid-state LMBs.

## Author contributions

X.-M. Z. conceived and designed this project. J.-Q. S. and Y.-L. S. performed the experiments. C.-T. H. carried out the DFT calculation. J.-Q. S., Y.-L. S., C. Z., X. L., Z. Q., Y. L. and X.-M. Z. analyzed the data, J.-Q. S. and X.-M. Z. wrote and revised the article.

## Conflicts of interest

There are no conflicts to declare.

## Acknowledgements

We are sincerely thankful for the financial support of the Natural Science Foundation of China (22271211 and 91961201), 1331 Project of Shanxi Province, and the Natural Science Foundation of Shanxi Province (20210302124055).

## References

1 J. M. Tarascon and M. Armand, Issues and challenges facing rechargeable lithium batteries, *Nature*, 2001, **414**, 359.
2 S. Chu and A. Majumdar, Opportunities and challenges for a sustainable energy future, *Nature*, 2012, **488**, 294.

 

3 J. W. Choi and D. Aurbach, Promise and reality of post-lithium-ion batteries with high energy densities, *Nat. Rev. Mater.*, 2016, **1**, 16013.
4 W. Xu, J. Wang, F. Ding, X. Chen, E. Nasybulin, Y. Zhang and J.-G. Zhang, Lithium metal anodes for rechargeable batteries, *Energy Environ. Sci.*, 2014, **7**, 513.
5 X.-B. Cheng, R. Zhang, C.-Z. Zhao and Q. Zhang, Toward safe lithium metal anode in rechargeable batteries: a review, *Chem. Rev.*, 2017, **117**, 10403.
6 M. D. Tikekar, S. Choudhury, Z. Tu and L. A. Archer, Design principles for electrolytes and interfaces for stable lithium-metal batteries, *Nat. Energy*, 2016, **1**, 16114.
7 D. Lin, Y. Liu and Y. Cui, Reviving the lithium metal anode for high-energy batteries, *Nat. Nanotechnol.*, 2017, **12**, 194.
8 H. Zhang, C. Li, M. Piszcz, E. Coya, T. Rojo, L. M. Rodriguez-Martinez, M. Armand and Z. Zhou, Single lithium-ion conducting solid polymer electrolytes: advances and perspectives, *Chem. Soc. Rev.*, 2017, **46**, 797.
9 R. Bouchet, S. Maria, R. Meziane, A. Aboulaich, L. Lienafa, J.-P. Bonnet, T. N. T. Phan, D. Bertin, D. Gigmes, D. Devaux, R. Denoyel and M. Armand, Single-ion BAB triblock copolymers as highly efficient electrolytes for lithium-metal batteries, *Nat. Mater.*, 2013, **12**, 452.
10 J. C. Bachman, S. Muy, A. Grimaud, H.-H. Chang, N. Pour, S. F. Lux, O. Paschos, F. Maglia, S. Lupart, P. Lamp, L. Giordano and Y. Shao-Horn, Inorganic solid-state electrolytes for lithium batteries: mechanisms and properties governing ion conduction, *Chem. Rev.*, 2016, **116**, 140.
11 V. Thangadurai, S. Narayanan and D. Pinzaru, Garnet-type solid-state fast Li ion conductors for Li batteries: critical review, *Chem. Soc. Rev.*, 2014, **43**, 4714.
12 R. Murugan, V. Thangadurai and W. Weppner, Fast lithium ion conduction in garnet-type $Li_7La_3Zr_2O_{12}$, *Angew. Chem., Int. Ed.*, 2007, **46**, 7778.
13 F. Mizuno, A. Hayashi, K. Tadanaga and M. Tatsumisago, Highly ion-conductive crystals precipitated from $Li_2S$–$P_2S_5$ glasses, *Adv. Mater.*, 2005, **17**, 918.
14 N. Kamaya, K. Homma, Y. Yamakawa, M. Hirayama, R. Kanno, M. Yonemura, T. Kamiyama, Y. Kato, S. Hama, K. Kawamoto and A. Mitsui, A lithium superionic conductor, *Nat. Mater.*, 2011, **10**, 682.
15 Q. Ma, H. Zhang, C. Zhou, L. Zheng, P. Cheng, J. Nie, W. Feng, Y.-S. Hu, H. Li, X. Huang, L. Chen, M. Armand and Z. Zhou, Single lithium-ion conducting polymer electrolytes based on a super-delocalized polyanion, *Angew. Chem., Int. Ed.*, 2016, **55**, 2521.
16 L. Shen, H.-B. Wu, F. Liu, L. Brosmer Jonathan, G. Shen, X. Wang, I. Zink Jeffrey, Q. Xiao, M. Cai, G. Wang, Y. Lu and B. Dunn, Creating lithium-ion electrolytes with biomimetic ionic channels in metaleorganic frameworks, *Adv. Mater.*, 2018, **30**, 1707476.
17 B. M. Wiers, M.-L. Foo, N. P. Balsara and J. R. Long, A solid lithium electrolyte via addition of lithium isopropoxide to a metal–organic framework with open metal sites, *J. Am. Chem. Soc.*, 2011, **133**, 14522.
18 S. S. Park, Y. Tulchinsky and M. Dincă, Single-ion $Li^+$, $Na^+$, and $Mg^{2+}$ solid electrolytes supported by a mesoporous anionic Cu-azolate metal-organic framework, *J. Am. Chem. Soc.*, 2017, **139**, 13260.
19 R. Ameloot, M. Aubrey, B. M. Wiers, A. P. Gómora-Figueroa, S. N. Patel, N. P. Balsara and J. R. Long, Ionic conductivity in the metal-organic framework UiO-66 by dehydration and insertion of lithium tert-butoxide, *Chem. – Eur. J.*, 2013, **19**, 5533.
20 J. Jiang, F. Gándara, Y.-B. Zhang, K. Na, O. M. Yaghi and W. G. Klemperer, Superacidity in sulfated metal-organic framework-808, *J. Am. Chem. Soc.*, 2014, **136**, 12844.
21 S. Ma, L. Shen, Q. Liu, W. Shi, C. Zhang, F. Liu, J. A. Baucom, D. Zhang, H. Yue, H. B. Wu and Y. Lu, Class of solid-like electrolytes for rechargeable batteries based on metal-organic framework infiltrated with liquid electrolytes, *ACS Appl. Mater. Interfaces*, 2020, **12**, 43824.
22 W. Xu, X. Pei, C. S. Diercks, H. Lyu, Z. Ji and O. M. Yaghi, A metal-organic framework of organic vertices and polyoxometalate linkes as solid-state electrolyte, *J. Am. Chem. Soc.*, 2019, **141**, 17522.
23 K. Nath, A. Bin Rahaman, R. Moi, K. Maity and K. Biradha, Porous Li-MOF as a solid-state electrolyte: exploration of lithium ion conductivity through bio-inspried ionic channels, *Chem. Commun.*, 2020, **56**, 14873.
24 I. S. Ramsey, Y. Mokrab, I. Carvacho, Z. A. Sands, M. S. P. Sansom and D. E. Clapham, An aqueous $H^+$ permeation pathway in the voltage-gated proton channel Hv1, *Nat. Struct. Mol. Biol.*, 2010, **17**, 869.
25 P. Ji, J. B. Solomon, Z. Lin, A. Johnson, R. F. Jordan and W. Lin, Transformation of metal-organic framework secondary building units into hexanuclear Zr-alkyl catalysts for ethylene polymerization, *J. Am. Chem. Soc.*, 2017, **139**, 11325.
26 H. Furukawa, F. Gándara, Y.-B. Zhang, J. Jiang, W. L. Queen, M. R. Hudson and O. M. Yaghi, Water adsorption in porous metal-organic frameworks and related materials, *J. Am. Chem. Soc.*, 2014, **136**, 4369.
27 S. Y. Moon, Y. Liu, J. T. Hupp and O. K. Farha, Instantaneous hydrolysis of nerve-agent simulants with a six-connected zirconium-based metal–organic framework, *Angew. Chem., Int. Ed.*, 2015, **54**, 6795.
28 J.-L. Pascal and F. Favier, Inorganic perchlorato complexes, *Coord. Chem. Rev.*, 1998, **178–180**, 865.
29 K. Xu, Nonaqueous liquid electrolytes for lithium-based rechargeable batteries, *Chem. Rev.*, 2004, **104**, 4303.
30 H. Wu, Y. Cao, H. Su and C. Wang, Tough gel electrolyte using double polymer network design for the safe, stable cycling of lithium metal anode, *Angew. Chem., Int. Ed.*, 2018, **57**, 1361.
31 Y. Du, H. Yang, J. M. Whiteley, S. Wan, Y. Jin, S.-H. Lee and W. Zhang, Ionic covalent organic frameworks with spiroborate linkage, *Angew. Chem., Int. Ed.*, 2016, **55**, 1737.
32 M. Watanabe, H. Tokuda and S. Muto, Anionic effect on ion transport properties in network polyether electrolytes, *Electrochim. Acta*, 2001, **46**, 1487.

33 S. Feng, D. Shi, F. Liu, L. Zheng, J. Nie, W. Feng, X. Huang, M. Armand and Z. Zhou, Single lithium-ion conducting polymer electrolytes based on poly[(4-styrenesulfonyl)(trifluoromethanesulfonyl)imide] anions, *Electrochim. Acta*, 2013, **93**, 254.

34 L. Porcarelli, A. S. Shaplov, M. Salsamendi, J. R. Nair, Y. S. Vygodskii, D. Mecerreyes and C. Gerbaldi, Single-ion block copoly(ionic liquid)s as electrolytes for all-solid state lithium batteries, *ACS Appl. Mater. Interfaces*, 2016, **8**, 10350.

35 Q. Ma, Y. Xia, W. Feng, J. Nie, Y.-S. Hu, H. Li, X. Huang, L. Chen, M. Armand and Z. Zhou, Impact of the functional group in the polyanion of single lithium-ion conducting polymer electrolytes on the stability of lithium metal electrodes, *RSC Adv.*, 2016, **6**, 32454.

36 S. Bai, Y. Sun, J. Yi, Y. He, Y. Qiao and H. Zhou, Impact of the functional group in the polyanion of single lithium-ion conducting polymer electrolytes on the stability of lithium metal electrodes, *Joule*, 2018, **2**, 2117.



 